Anatomical and principal axes are not aligned in the torso: considerations for users of geometric modelling methods

CHOPPIN, Simon <http://orcid.org/0000-0003-2111-7710>, CLARKSON, Sean, BULLAS, Alice <http://orcid.org/0000-0003-2857-4236>, THELWELL, Michael <http://orcid.org/0000-0003-0145-0452>, HELLER, Ben and WHEAT, Jon

Anatomical and principal axes are not aligned in the torso: considerations for users of geometric modelling methods.

Simon Choppin[1*], Sean Clarkson[1], Alice Bullas[1], Michael Thelwell[1], Ben Heller[1], Jon Wheat[1]

1 Sport and Physical Activity Research Centre, Sheffield Hallam University, Sheffield, UK

* Corresponding Author: s.choppin@shu.ac.uk; 0114 225 5717;

Keywords:

3D Imaging; Body Segment Inertial Parameters; Inverse Dynamics; Geometric Modelling; Principal Axes

Word Count (Introduction – Conclusions): 4,000

Abstract

The accuracy and accessibility of methods to calculate body segment inertial parameters are a key concern for many researchers. It has recently been demonstrated that the magnitude and orientation of principal moments of inertia are crucial for accurate dynamic models. This is important to consider given that the orientation of principal axes is fixed for the majority of geometric and regression body models. This paper quantifies the effect of subject specific geometry on the magnitude and orientation of second moments of volume in the trunk segment. The torsos of 40 male participants were scanned using a 3D imaging system and the magnitude and orientation of principal moments of volume were calculated from the resulting geometry. Principal axes are not aligned with the segment co-ordinate system in the torso segment, with mean Euler angles of 11.7, 1.9 and 10.3 in the ZXY convention. Researchers using anatomical modelling techniques should try and account for subject specific geometry and the mis-alignment of principal axes. This will help to reduce errors in simulation by mitigating the effect of errors in magnitude of principal moments.

Introduction

Body segment inertial parameters (BSIPs) are vital for biomechanical analyses that calculate forward- or inverse- dynamics of human movement (Hatze, 2002; Nagano et al., 2000) (inverse dynamics are sensitive to BSIPs primarily in high-acceleration movements such as the golf swing (Domone, 2014)). The accuracy and accessibility of methods to calculate BSIPs are, therefore, a key concern for many researchers. Medical imaging technologies that can be used to obtain gold-standard, subject-specific BSIPs (Cheng et al., 2000; Pearsall et al., 1996; Wicke & Dumas, 2008) remain inaccessible for many researchers. As a result, many in the community rely on datasets and models to calculate BSIPs from a small number of anthropometric measurements. The methods fall into two categories: 1) regression techniques estimate an individual's BSIP values through the application of equations to measurements of segment lengths and/or body weight and/or height (Yeadon & Morlock, 1989), 2) geometric methods approximate segments as a series of scaled 3D shapes, the BSIPs are then calculated using appropriate mathematical formulae and density values (Jensen, 1978; Wicke et al., 2009; Yeadon, 1990). Geometric methods better account for individual variation in volumetric proportion and distribution compared to regression techniques. However, the datasets on which regression models are based, and on which geometric methods are validated, have been relatively homogenous in terms of sex and age compared to the variability observed in the total population. The specifics of BSIP estimations have sustained interest from the research community for many decades (Challis, 1999; de Leva, 1996; Dumas et al., 2007; Durkin & Dowling, 2003; M. M. Rossi et al., 2016; Yeadon & Morlock, 1989).

This paper focuses on the magnitude of moments of inertia, centre of mass location and orientation of principal axes. Rossi et al. (M. M. Rossi et al., 2016) recently showed the importance of moments of inertia and quantified the effect of errors in the magnitude and orientation of principal moments. The motion of a cylinder was tracked in three dimensions and also simulated using forward dynamics. The simulations introduced errors of up to 10% in the principal moments and up to 10° of misalignment in the principal axes. Errors were expressed as angular deviations between the dynamic simulation and recorded motion. Errors up to 10% in magnitude of principal moments of inertia resulted in root mean squared deviation angles ranging between 3.2° and 6.6°, and between 5.5° and 7.9° when lumped with errors of 10° in principal axes of inertia orientation.

When calculating BSIPs, errors in the magnitude of moments of inertia have been shown to be proportionally higher compared to other inertial parameters (mass, centre of mass position) (M. Rossi, Lyttle, & El-Sallam, 2013) and most methods do not allow subject-specific alignment of the principal axes. In regression-based studies, product moments of inertia are often acknowledged but not included in calculations (Chandler et al., 1975; Zatsiorsky & Seluyanov, 1983). Mcconville and Churchill (McConville et al., 1980), presented full inertial tensors which were made more applicable by Dumas et al. (Dumas et al., 2007) through a change in co-ordinate system. We are aware of only one geometric method in which the principal axes are not implicitly aligned with the anatomical axes (Jensen, 1978).Given the continued use of regression and geometric models there is a need to quantify the extent to which their use might affect the accuracy of biomechanical simulation.

To better account for individual variations in segment geometry, new methods of calculating BSIPs have been explored using 3D imaging technology (Bullas et al., 2016; S Clarkson et al., 2014, 2012; Sean Clarkson et al., 2015; Kordi et al., 2019). While anatomical landmarking and segmentation of the resulting geometry is not trivial, it promises a cost-effective way to account for individual differences in body shape and avoid the symmetrical assumptions of traditional geometric methods. However, the technology cannot determine tissue density and its distribution. Thus, any analysis must either assume a constant density, use a density profile function or restrict analysis to volumetric parameters. Previous research has shown that inertial parameters are more sensitive to variations in geometry than variations in density (Wicke & Dumas, 2010).

The study presented in this paper uses a 3D imaging system to quantify the effect of subject specific geometry on the magnitude and orientation of second moments of volume[1] in the trunk segment. It does so by making a comparison to a geometric modelling method, putting into context the work of Rossi et al. (M. M. Rossi et al., 2016). This will allow users of geometric modelling methods to quantify the likely magnitude of errors resulting from their use in simulation.

[1] In this paper we will mostly disregard density information and consider the following body segment volume parameters (BSVPs): volume, centre of volume and second moment of volume.

Methods

Participants

Forty-one male participants (Mass 77.3 ± 9.1 Kg, stature 1.81 ± 0.06 m, BMI 23 ± 2) volunteered to take part in the study and provided written informed consent. Participants were recreationally active and able to stand in a stationary, upright position. Ethical approval was granted by our university Research Ethics Committee.

The profile of each participant's torso was obtained using two methods: geometric modelling and 3D imaging.

Yeadon's stadium solids (Yeadon, 1990) were used as the geometric method due to their wide application and relative complexity. Yeadon's method demonstrated low overall error compared to other methods of calculating BSIPs (M. Rossi, Lyttle, & El-Sallam, 2013) and is still being developed and utilised by researchers (Dembia et al., 2015).The regions of interest and corresponding stadium solids are shown in Figure 2.

Imaging system

The 3D imaging system was developed using consumer-level depth cameras and its accuracy and repeatability has been validated in previous studies (Bullas et al., 2016; Sean Clarkson et al., 2015). It comprised four depth cameras (Microsoft Kinect version 1, Microsoft Corporation, Redmond, USA) mounted in a vertical orientation (Figure 1a). The depth cameras were affixed to four tripods, and located 0.8 m from the centre of a 0.4 m x 0.4 m x 1.2 m capture volume.

A single computer running custom software (Kinanthroscan, Sheffield Hallam University, UK) was used to control the depth cameras, perform calibration, and capture scans. The scan time was ~1 second.

Manual measurement protocol

Upon arrival, participants were asked to remove clothing from their upper body and change into a pair of close fitting, non-compressive shorts. The stature and weight of each participant were recorded using a stadiometer and digital scales. Anatomical landmarks (Figure 2) were palpated and marked by an International Society for the Advancement of Kinanthropometry (ISAK) level one qualified practitioner. Girth and breadth measurements were taken at the level of each set of landmarks using anatomical tape and digital callipers (Kennedy, Leicester, UK), respectively. The length of each segment was also measured using the digital callipers. Each measurement was repeated three times and mean values taken. These measurements were used in conjunction with Yeadon's formulae (Yeadon 1990b) to model the three stadium solids representing the trunk and their related inertial parameters. Throughout the manual measurement process, the same body control techniques as those used for the scanning process, discussed below, were adopted by the participant.

Imaging protocol

After manual measurement and palpation, participants entered the calibrated scanning volume. Anatomical markers were used for segmentation and to generate a local segment co-ordinate system. Each participant was scanned three times. A break of one minute was interspersed between each scan during which the participant left and re-entered the calibrated volume. Footprint markers in the centre of the capture volume ensured participants stood in the same location for each scan (Kirby et al., 1987). Participants were asked to adopt a modified version of the scanning pose defined by ISO 20685-1 (ISO, 2018), arms were held out from the torso at an angle of approximately 45° to ensure underarm areas were visible in the scans.

Two tripods were used as hand supports were used to limit involuntary movement during scanning. The height and position of the supports were adjusted prior to scanning and a goniometer ensured the participant’s arms were at 45°. Participants were asked to hold their breath at the end of the natural expiration cycle to reduce movement (Schranz et al., 2010).

Imaging post processing and volume calculation

After collection, each 3D scan was manually digitised by a single operator using kinanthroscan software. Four markers were digitised on each scan, both of the ASIS markers and both of the nipple markers. An anatomical axes system was created in agreement with ISB recommendations (Wu et al., 2005) such that the x-axis ran posterior-anterior, the y-axis ran inferior-superior and the z-axis ran from the participants’ left-right (figure 3). The system was set-up as follows (referring to figure 3):

- Two markers were created: $M1^*$ and $M4^*$, as the midpoints of the vectors $\overrightarrow{M1M2}$ and $\overrightarrow{M4M5}$
- Two horizontal vectors (perpendicular to $\overrightarrow{M1M2}$ and $\overrightarrow{M4M5}$) were projected from $M1^*$ and $M4^*$. The locations at which these vectors intersected the surface of the scan formed markers M3 and M6.
- The **origin** O was located at the midpoint of vector $\overrightarrow{M1^*M3}$
- The **x-axis** X was initially defined as the vector $\overrightarrow{OM1^*}$
- The **y-axis** Y was defined as the vector from the origin to the midpoint of $\overrightarrow{M4^*M6}$
- The **z-axis** Z was defined as the cross product of X and Y: $Z = X \times Y$

- The **x-axis** was re-defined (to ensure an orthogonal co-ordinate set) as the cross product of Y and Z: $X = Y \times Z$

Volume, centre of volume position and second moments of volume were calculated the scan data, which consisted of a series of unconnected data points. The scan was constrained to only include data points relating to the torso segment. The torso's scan data were split along the y-axis into 2 mm 'slices' (the minimum permissible size to ensure features were accurately represented). A cubic spline was fitted through each slice (as a representation of its perimeter) and used to calculate the inertial parameters.

Calculation of volume

The volume of the segment was calculated by summing the volumes of each slice which was calculated by multiplying the area within its perimeter by the slice's height (2 mm). The area within a slice's perimeter was calculated by dividing the space into 360 triangles with the apex of each located at the centroid -- the area of each triangle was summed.

Calculation of the 2nd moments of volume

The moments of volume were calculated using Crisco and McGovern's application of Green's Theorem (Crisco & McGovern, 1998). The spline representing the perimeter was sampled at 360 points for each of the *S* slices. With the local *x*, *y* and *z* coordinates of each point the moments of inertia can be calculated from:

$$I_{xx} = \sum_{s=1}^{S} dy \times \sum_{p=1}^{360} \left(u(s,p) \cdot y(s)^2 \cdot dz(s,p) - \frac{1}{3} v(s,p)^3 \cdot dx(s,p) \right)$$

$$I_{yy} = \sum_{s=1}^{S} dy \times \sum_{p=1}^{360} \left(\frac{1}{3} u(s,p)^3 \cdot dz(s,p) - \frac{1}{3} v(s,p)^3 \cdot dx(s,p) \right)$$

$$I_{zz} = \sum_{s=1}^{S} dy \times \sum_{p=1}^{360} \left(\frac{1}{3}u(s,p)^3 \cdot dz(s,p) - y(s)^2 \cdot v(s,p) \cdot dx(s,p)\right)$$

where $u(s,p) = \frac{x(s,p+1)+x(s,p)}{2}$, $v(s,p) = \frac{z(s,p+1)+z(s,p)}{2}$

$y(s) = 0.002(s-1) + 0.001$

$dx(s,p) = x(s,p+1) - x(s,p);\qquad dy = 0.002;\quad dz(s,p) = z(s,p+1) - z(s,p)$

The y co-ordinate was set to the midpoint position of the slice being analysed.

Calculation of centre of volume position

In a similar way, the centre of volume location was calculated in the local *x*, *y*, and *z* directions by:

$$c_x \cdot V = \sum_{p=1}^{360} \left(\frac{1}{2}u(s,p)^2 \cdot dz(s,p)\right)$$

$$c_y \cdot V = \sum_{p=1}^{360} \left(\frac{1}{2}u(s,p) \cdot dz(s,p) - \frac{1}{2}v(s,p) \cdot dx(s,p)\right)$$

$$c_z \cdot V = -\sum_{p=1}^{360} \left(\frac{1}{2}v(s,p)^2 \cdot dx(s,p)\right)$$

Equivalent inertial parameters were obtained from the geometric representations using the manual measurements in conjunction with Yeadon's formulae (Yeadon 1990b). Yeadon's original paper details the equations so they aren't repeated here, they have also recently been implemented in Python code that is available as open source (Dembia et al., 2015). It should be noted that density was disregarded in our calculations (the equivalent of setting ρ=1). The parallel axis theorem was used to combine the separate stadium solids and to translate the origin to the centre of the lower face of the lower segment (the equivalent position to the 3D imaged torso). When calculating geometric parameters the height of the upper and lower trunk were adjusted so that the overall height of the torso matched that of the 3D scan. This was to prevent differences in a single dimension dominating differences in volumetric parameters.

Data analysis

The agreement between volume and second moments of volume estimates were assessed using limits of agreement (LOA) (Bland & Altman 1986). The repeatability of measurement of each technique was assessed by calculating the repeatability coefficient (Bland & Altman, 2003) for volume, centre of volume and second moment of volume.

Geometric differences between each technique were assessed by calculating the relative orientations of the principal axes, calculated as ‘ZXY’ Euler angles.

Simulation

To assess the effect of the differences in inertial properties, simulations were set-up in Opensim (v. 4.1, simtk.org, Stanford, CA) via the Matlab (v. 9.9.0, The Math Works, Natick, Massachusetts) Application Programming Interface (API).

We simulated a single, unconnected and rigid segment in two separate movements: a free and a driven motion.In the free motion the segment was freely supported and rotated at a speed of 2π rad/s about the z-axis. In the driven motion a torque of 1 Nm acted about the segment’s y-axis for 0.1 s. The segment was fixed with a ball-joint at its anatomical origin (the lower extremity).

Inertial properties were calculated by multiplying volumetric parameters by a density value of 0.97. This is an average of the values used by Yeadon (Yeadon, 1990) for the thorax and abdomen (0.92 and 1.01

respectively) that were originally taken from Dempster (Dempster, 1955). This resulted in two sets of data, a set of parameters obtained using the geometric method and a set of parameters obtained using the 3D imaging method.

Both scenarios were run with each set of inertial parameters, angular positions and velocities of the geometric data set were compared with those of the 3D imaging data set. This was done for each participant, resulting in 160 simulations in total. The following comparisons were made:

1) The free motion simulations were run for 1 second. The angular deviation (from an axis-angle representation) between segment orientations (geometric and 3D imaging) were assessed for each participant.
2) The driven motion simulations were run for 0.1 seconds to assess:
    a) differences in rotational speed between geometric and 3D imaging segments for each participant.
    b) the angle between the axes of rotation for geometric and 3D imaging segments for each participant.

Results

Due to problems during data collection, data relating to one participant were removed from this study. Therefore, the results relate to forty participants. The mean volume, centre of volume and principal moments for each participant are provided as supplementary material (with repeatability coefficients) and are summarised in table 1.

Agreement between methods

Figure 4 shows the agreement between scan-derived and Yeadon-derived volume, assessed using limits of agreement (accounting for the fact three repeats were taken for each participant rather than single measurements (Bland & Altman, 1999)).

The volume calculated using the scan method agreed with the geometric method to -0.22 ± 1.58 litres. Limits of agreement were -1.80 litres and 1.35 litres or -9.96% and 7.39% of average torso volume. Volume estimates calculated using the geometric method tend to be 0.22 litres higher than using the geometric method but this systematic difference is small compared to the random differences between them. A systematic difference of -1.3% and a mean absolute difference of 3.2% was observed.

Figure 5 shows the agreement between scan-derived and Yeadon-derived second moments of volume along the principal axes. Along the first principal axis the scan method agreed with the geometric method to -0.87 ± 2.76 m^{5}x10^{-5}. The limits of agreement were –3.63 m^{5}x10^{-5} to 1.89 m^{5}x10^{-5}. Along the second principal axis the scan method agreed with the geometric method to -1.68 ± 2.80 m^{5}x10^{-5}. The limits of agreement were -4.48 m^{5}x10^{-5} to 1.12 m^{5}x10^{-5}. Along the third principal axis the scan method agreed with the geometric method to 0.34 ± 2.39 m^{5}x10^{-5}. The limits of agreement were -2.05 m^{5}x10^{-5} to 2.73 m^{5}x10^{-5}. Systematic differences of -3.2%, -7.7% and 1.9% and mean absolute differences of 3.9%, 8.6% and 5.7% around the first, second and third principal axes were observed between the two methods.

Repeatability of Measurement

The geometric method was marginally more repeatable than the scanning method regarding volume, with a 95% probability that 2 measurements will be within 0.96 litres as opposed to 1.12 litres with scanning.

Repeatability of the second moment of volume was similar in magnitude around the second principal axis for both methods. The geometric method had better repeatability around the first and third principal axes. Coefficients of repeatability were 3.00, 2.60 and 1.80 m^5x10^5 (10.7%, 11.8% and 10.0% of mean values) for scanning compared to 2.36, 2.62 and 1.19 m^5x10^5 (8.8%, 12.6% and 6.26% of mean values) for the geometric method.

Centre of Volume

In the scan method, the centre of volume was positioned anterior to the origin of the local coordinate system in all cases (mean = 22.2 mm, range 11.2-29.8 mm). The scanned segments were approximately symmetrical in the frontal plane (with a mean medio-lateral (z) position of 0.5 mm, range -7.3-4.7 mm). Mean centre of mass position along the y-axis was similar between scanning and geometric methods (159.2 and 160.1 mm for scanning and geometric methods respectively).

Principal Axes

In the geometric method the 1st, 2nd and 3rd principal moments were, by default, aligned with the sagittal (x), transverse (z) and vertical (y) axes respectively. With the scanning method, the principal moments were not restricted by the calculation method and alignment could vary from with the anatomical axes-system. The discrepancy in alignment between the two methods was expressed as Euler angles in the ZXY convention (table 2). The first Euler angle was, on average 11.8° which reflects the tendency of the third principal axis to be directed towards the superior anterior aspect of the torso when using the 3D imaging method. The third Euler angle had a mean of 10.3° but a median of 4.3° due to a small number of large values. In two participants the 1st and 2nd principal moments were switched in comparison to the geometric method, this corresponded to a third Euler angle of around 90 degrees. The repeatability coefficient of the third Euler angle had a mean of 13.3° but a median of 4.5°. This discrepancy is due to three individuals having very poor repeatability (14, 22, 35).

Simulation Results

Figure 6 shows the range of differences obtained during rigid body simulation and the relationship with inertial properties.

As the difference in moment of inertia about the local y-axis increased (between the geometric and 3D imaging methods) the rotational speed of the segment in the driven motion decreased, figure 6a (r = -0.99). The magnitude of differences in I_Y observed in this study resulted in differences of angular velocity between -16.2% and 21.0%.

Scanned centre of mass locations away from a segment's y-axis resulted in differences in the angular velocity vector orientation (compared to the geometric simulation). Angular difference increased as the centre of mass moved away from the y-axis (in the local x-direction, r= 0.92) as shown in figure 6b. The centre of mass locations observed in this study resulted in deviations in the angular velocity vector between 4.3° and 9.6°.

The presence of product moments of inertia (a misalignment between the principal axes and anatomical axes) resulted in off-axis rotations during the free rotation. Deviation angles between geometric and 3D imaging segments are illustrated in figure 6c and they are correlated with the magnitude of product moments of inertia (specifically, I_{XZ} and I_{YZ} as the initial rotation is about the local z-axis, r = 0.81). The inertial properties observed in this study resulted in deviation angles between 0.6° and 27.3°.

Discussion

Geometric modelling methods use a series of anthropometric measurements to create a (most often symmetrical) representation of the torso. In reality, the presence of off-centre mass violates symmetrical assumptions –no individual's principal and anatomical axes were aligned in our study, with mean Euler angles (ZXY) of 11.65, 1.93 and 10.31° between the two. The torso segment was chosen in this study as it is large and central to many biomechanical analyses (MacKenzie & Sprigings, 2009; Nesbit, 2005; Ren et al., 2008; Winter, 1995). As a segment, it is also likely to violate symmetrical assumptions due to varying amounts of off-centre mass in the form of adipose tissue. Future studies that adopt a similar approach should consider using the acromion process of the shoulders as opposed to the nipples for anatomical markers – this will allow the research include female participants.

Many geometric modelling methods have been developed and assessed using young, athletic participants (M. Rossi, Lyttle, & El-Sallam, 2013; Yeadon, 1990). This study is similar, with a mean BMI of 23 (full range 19 – 29). All users of modelling methods should assume that principal and anatomical axes do not align in the torso segment, regardless of the participant population. However, biomechanical analyses considering overweight populations should pay particular attention to the method used to calculate individual BSIPs. The presence of atypical geometry that presents off-centre mass is more likely and researchers should anticipate larger deviations than those presented here. Given the random variation in orientation and magnitude differences observed in this study, systematically correcting principal moments is not possible and users should aim to use more sophisticated methods than geometric modelling for obtaining BSIPs of the torso segment.

The simulated motions were included to highlight how differences in the magnitudes of principal moments of inertia, a centre of mass lying away from the segments' y-axis and a mis-alignment between principal and anatomical axes manifest in altered dynamic behaviour. In reality, the simulations will be more complex than the simple cases presented here. While the simulated motions are illustrative, the differences in inertial properties between methods are representative because they are based on the results presented in this study. It should be noted that during the simulation we used a single, uniform density for all cases. Future studies with sophisticated models assessing representative motions should aim to use realistic density profiles.

Of the three comparisons made in figure 6, the position of the centre of mass should be considered carefully, it is the only one of three comparisons which does not have differences in simulation close to zero. Even with participants that may be close to the 'geometric ideal' off centre mass is always present and results in differences in simulation that shouldn't be dismissed. If researchers have the opportunity or means, they should attempt to account for centre of mass position as a priority.

Future work should attempt to fully quantify the effect of errors in BSIP errors in a realistic simulation – for example, in a high-acceleration driven motion such as a golf-swing or a free aerial motion such as a front flip.

Agreement in volume between the two methods was good, with a low (≈1% of mean) systematic error and limits of agreement within 10% of the mean volume; mean differences were similar to other agreement studies examining the Yeadon method (M. Rossi, Lyttle, El-Sallam, et al., 2013). While the strength of agreement was lower with second moments of volume, the mean errors in this study are lower than those recorded previously when comparing geometric methods against techniques using dual X-ray absorptiometry (DXA) (M. Rossi, Lyttle, & El-Sallam, 2013). A major difference in the previous study (M. Rossi, Lyttle, & El-Sallam, 2013) was the specific density profiles afforded by the DXA scan (compared to the uniform density of the Yeadon model). In addition, realistic body models should contain non-rigid elements. This study assumed rigid bodies. The effects of geometry on inertial (volumetric) properties was the primary focus of this paper and non-rigid modelling was beyond the scope of this work. Future work would benefit from combining the realistic geometries obtained by 3D imaging with non-rigid modelling. This could help to quantify the magnitude of off-centre masses in the abdomen and predict how it may deform under load.

Conclusions

- The participant specific advantages of geometric modelling methods are lost when symmetric assumptions are violated. Off-set mass was observed for every participant in this study.
- One should expect principal axes to be misaligned with anatomical axes when assessing the torso segment.
- Low-cost 3D scanning techniques offer a potential solution when more sophisticated medical imaging (such as DXA) is unavailable, however, the effect of variable density is still not accounted for.

Conflicts of Interest

The authors declare they have no conflicts of interest.

References

Bland, J. M., & Altman, D. G. (1999). Measuring agreement in method comparison studies - Statistical Methods in Medical Research | SwetsWise Online Content. *Statistical Methods in Medical Research*, *8*, 135–160. https://www-swetswise-com.libproxy.ucl.ac.uk/swoc-web/linkingDetails.html?openURL=false&issn=0962-2802&eissn=0962-2802&volume=8&issue=2&page=135

Bland, J. M., & Altman, D. G. (2003). Applying the right statistics: Analyses of measurement studies. *Ultrasound in Obstetrics and Gynecology*, *22*(1), 85–93. https://doi.org/10.1002/uog.122

Bullas, A. M., Choppin, S., Heller, B., & Wheat, J. (2016). Validity and repeatability of a depth camera-based surface imaging system for thigh volume measurement. *Journal of Sports Sciences*, *34*(20), 1998–2004. https://doi.org/10.1080/02640414.2016.1149604

Challis, J. H. (1999). Precision of the Estimation of Human Limb Inertial Parameters. *Journal of Applied Biomechanics*, *15*(4), 418–428. https://doi.org/10.1123/jab.15.4.418

Chandler, R. F., Clauser, C. E., McConville, J. T., Reynolds, H. M., & Young, J. W. (1975). Investigation of inertial properties of the human body. In *National Highway Traffic Safety Administration*. https://doi.org/10.1017/CBO9781107415324.004

Cheng, C. K., Chen, H. H., Chen, C. S., Lee, C. L., & Chen, C. Y. (2000). Segment inertial properties of Chinese adults determined from magnetic resonance imaging. *Clinical Biomechanics*, *15*, 559–566. https://doi.org/10.1016/S0268-0033(00)00016-4

Clarkson, S, Choppin, S. B., Hart, J., Heller, B., & Wheat, J. S. (2012). Calculating Body Segment Inertia Parameters from a Single Rapid Scan Using the Microsoft Kinect. *3rd International Conference and Exhibition on 3D Body Scanning*, *October*, 153–163.

Clarkson, S, Wheat, J. S., Heller, B., & Choppin, S. B. (2014). Assessing the Suitability of the Microsoft Kinect for Calculating Person Specific Body Segment Parameters. *4th IEEE Workshop on Consumer Depth Cameras for Computer Vision*.

Clarkson, S, Wheat, J. S., Heller, B., Webster, J., & Choppin, S. B. (2013). Distortion Correction of Depth Data from Consumer Depth Cameras. In N. D'Apuzzo (Ed.), *4th International Conference and Exhibition on 3D Body Scanning*.

Clarkson, Sean, Wheat, J., Heller, B., & Choppin, S. (2015). Assessment of a Microsoft Kinect-based 3D scanning system for taking body segment girth measurements: a comparison to ISAK and ISO standards. *Journal of Sports Sciences*, 1–9. https://doi.org/10.1080/02640414.2015.1085075

Crisco, J. J., & McGovern, R. D. (1998). Efficient calculation of mass moments of inertia for segmented homogeneous three-dimensional objects. *Journal of Biomechanics*, *31*(1), 97–101. http://www.ncbi.nlm.nih.gov/pubmed/9596545

de Leva, P. (1996). Adjustments to Zatsiorsky-Seluyanov's segment inertia parameters. *Journal of Biomechanics*, *29*(9), 1223–1230. https://doi.org/10.1016/0021-9290(95)00178-6

Dembia, C., Moore, J. K., & Hubbard, M. (2015). An object oriented implementation of the Yeadon human inertia model. *F1000Research*, *3*, 223. https://doi.org/10.12688/f1000research.5292.2

Dempster, W. T. (1955). Space requirements of the seated operator. *WADC Technical Report 55159*, *55*(WADC-55-159, AD-087-892), 55–159. http://www.mendeley.com/research/space-requirements-of-the-seated-operator/

Domone, S. (2014). *Validation and uncertainty of inverse dynamics analysis applied to high acceleration movements* [Sheffield Hallam University]. http://shura.shu.ac.uk/23508/1/10760405.pdf

Dumas, R., Chèze, L., & Verriest, J. P. (2007). Adjustments to McConville et al. and Young et al. body segment inertial parameters. *Journal of Biomechanics*, *40*(3), 543–553. https://doi.org/10.1016/j.jbiomech.2006.02.013

Durkin, J. L., & Dowling, J. J. (2003). Analysis of Body Segment Parameter Differences Between Four Human Populations and the Estimation Errors of Four Popular Mathematical Models. *Journal of Biomechanical Engineering*, *125*(4), 515. https://doi.org/10.1115/1.1590359

Hatze, H. (2002). The fundamental problem of myoskeletal inverse dynamics and its implications. *Journal of Biomechanics*, *35*(1), 109–115. http://www.ncbi.nlm.nih.gov/pubmed/11747889

ISO. (2018). *3-D scanning methodologies for internationally compatible anthropometric databases*.

Jensen, R. K. (1978). Estimation of the biomechanical properties of three body types using a photogrammetric method. *Journal of Biomechanics*, *11*(8–9), 349–358. https://doi.org/10.1016/0021-9290(78)90069-6

Kirby, R. L., Price, N. A., & MacLeod, D. A. (1987). The influence of foot position on standing balance. *Journal of Biomechanics*, *20*(4), 423–427. https://doi.org/10.1016/0021-9290(87)90049-2

Kordi, M., Haralabidis, N., Huby, M., Barratt, P. R., Howatson, G., & Wheat, J. S. (2019). Reliability and validity of depth camera 3D scanning to determine thigh volume. *Journal of Sports Sciences*, *37*(1), 36–41. https://doi.org/10.1080/02640414.2018.1480857

MacKenzie, S. J., & Sprigings, E. J. (2009). A Three-Dimensional Forward Dynamics Model of the Golf Swing. *Sports Engineering*, *11*, 165–175.

McConville, J. T., Clauser, C. E., Churchill, T. D., Cuzzi, J., & Kaleps, I. (1980). Anthropometric Relationships of Body and Body Segment Moments of Inertia. In *Report*. https://doi.org/10.1073/pnas.0710346105

Nagano, a, Gerritsen, K. G., & Fukashiro, S. (2000). A sensitivity analysis of the calculation of mechanical output through inverse dynamics: a computer simulation study. *Journal of Biomechanics*, *33*(10), 1313–1318. http://www.ncbi.nlm.nih.gov/pubmed/10899342

Nesbit, S. (2005). A three dimensional kinematic and kinetic study of the golf swing. *Journal of Sports Science and Medicine*, *4*, 499–519. http://jsportscimed.org/vol4/n4/17/v4n4-17pdf.pdf

Pearsall, D. J., Reid, J. G., & Livingston, L. A. (1996). Segmental inertial parameters of the human trunk as determined from computed tomography. *Annals of Biomedical Engineering*, *24*(2), 198–210. https://doi.org/10.1007/BF02667349

Ren, L., Jones, R. K., & Howard, D. (2008). Whole body inverse dynamics over a complete gait cycle based only on measured kinematics. *Journal of Biomechanics*, *41*, 2750–2759. https://doi.org/10.1016/j.jbiomech.2008.06.001

Rossi, M., Lyttle, A., & El-Sallam, A. (2013). Body segment inertial parameters of elite swimmers using DXA and indirect methods. *Journal of Sports Science and Medicine*, *12*, 761–775. http://jssm.org/vol12/n4/19/v12n4-19pdf.pdf

Rossi, M., Lyttle, A., El-Sallam, A., Benjanuvatra, N., & Blanksby, B. (2013). Body segment inertial parameters of elite swimmers using DXA and indirect methods. *Journal of Sports Science and Medicine*, *12*(4), 761–775.

Rossi, M. M., Alderson, J., El-Sallam, A., Dowling, J., Reinbolt, J., & Donnelly, C. J. (2016). A new validation technique for estimations of body segment inertia tensors: Principal axes of inertia do matter. *Journal of Biomechanics*, *49*(16), 4119–4123. https://doi.org/10.1016/j.jbiomech.2016.10.006

Schranz, N., Tomkinson, G., Olds, T., & Daniell, N. (2010). Three-dimensional anthropometric analysis: Differences between elite Australian rowers and the general population. *Journal of Sports Sciences*, *28*(5), 459–469. https://doi.org/10.1080/02640411003663284

Stewart, A., Marfell-Jones, M., Olds, T., & de Ridder, H. (2011). *International Standards for Anthropometric Assessment*.

Wicke, J., & Dumas, G. A. (2008). Estimating Segment Inertial Parameters Using Fan-Beam DXA. *Journal of Applied Biomechanics*, *24*(2), 180–184. https://doi.org/10.1123/jab.24.2.180

Wicke, J., Dumas, G. A., & Costigan, P. A. (2009). A comparison between a new model and current models for estimating trunk segment inertial parameters. *Journal of Biomechanics*, *42*(1), 55–60. https://doi.org/10.1016/j.jbiomech.2008.10.003

Wicke, J., & Dumas, G. a. (2010). Influence of the volume and density functions within geometric models for estimating trunk inertial parameters. *Journal of Applied Biomechanics*, *26*(1), 26–31. http://www.ncbi.nlm.nih.gov/pubmed/20147755

Winter, D. A. (1995). Human balance and posture control during standing and walking. *Gait and Posture*, *3*, 193–214. https://doi.org/10.1016/0966-6362(96)82849-9

Wu, G., Vanderhelm, F., Dirkjanveeger, H., Makhsous, M., Vanroy, P., Anglin, C., Nagels, J., Karduna, A., Mcquade, K., & Wang, X. (2005). ISB recommendation on definitions of joint coordinate systems of various joints for the reporting of human joint motion--Part II: shoulder, elbow, wrist and hand. *Journal of Biomechanics*, *38*(5), 981–992. https://doi.org/10.1016/j.jbiomech.2004.05.042

Yeadon, M. R. (1990). The simulation of aerial movement--II. A mathematical inertia model of the human body. *Journal of Biomechanics*, *23*(1), 67–74. http://www.ncbi.nlm.nih.gov/pubmed/2307693

Yeadon, M. R., & Morlock, M. (1989). The appropriate use of regression equations for the estimation of segmental inertia parameters. *Journal of Biomechanics*, *22*(6–7), 683–689. https://doi.org/10.1016/0021-9290(89)90018-3

Zatsiorsky, V., & Seluyanov, V. (1983). The mass and inertia characteristics of the main segments of the human body. In H. Matsui & K. Kobayashi (Eds.), *Biomechanics VIIIB* (Vol. 4B, pp. 1152–1159). Human Kinetics. http://scholar.google.com/scholar?hl=en&btnG=Search&q=intitle:The+mass+and+inertia+characteristics+of+the+main+segments+of+the+human+body.#0

Figures:

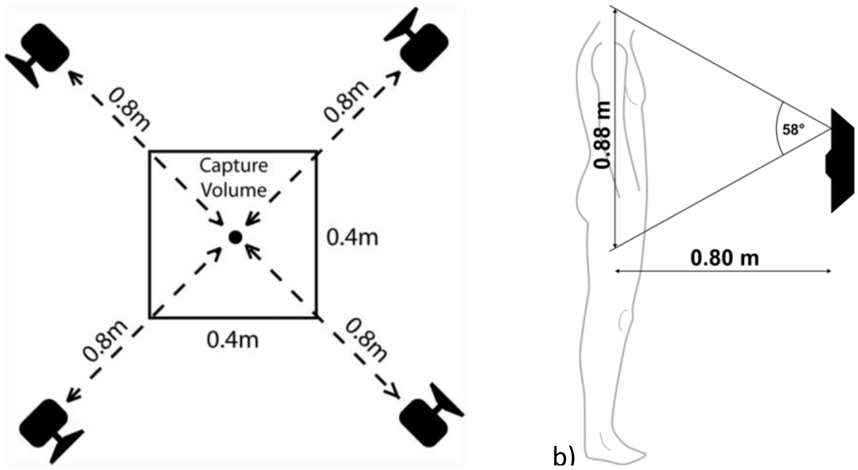

Figure 1. Overview of the Kinect scanning system; a) Layout of the scanning system; b) Scanning field of view.

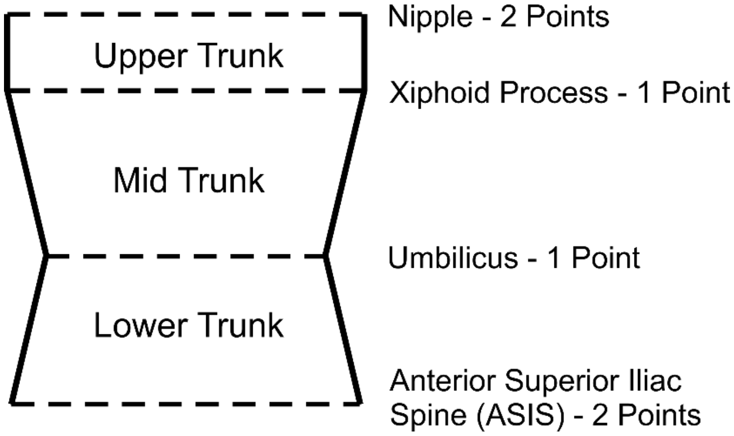

Figure 2. Anatomical landmarks and the segmentation process of the trunk.

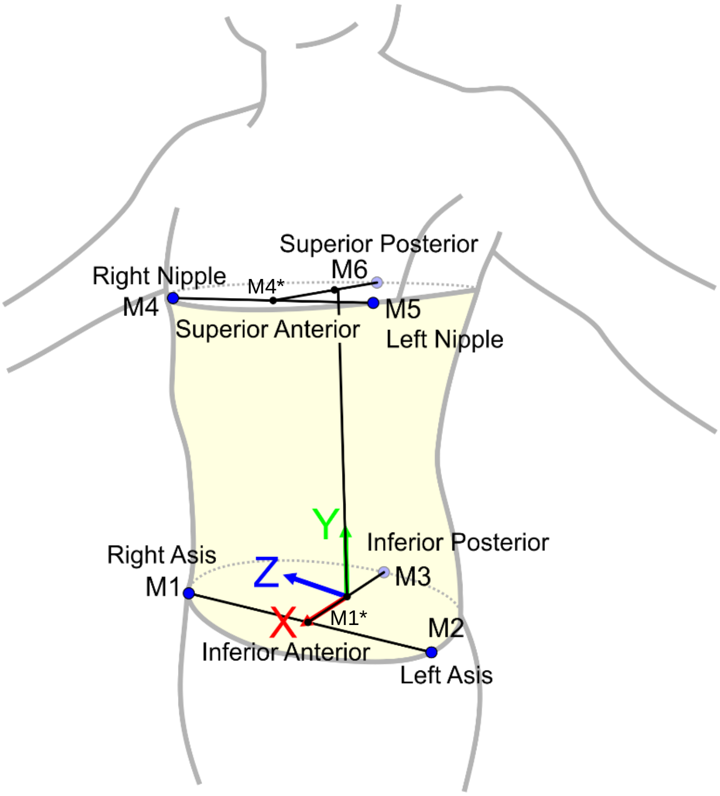

Figure 3. The marker set created for the 3D imaging as used to segment the torso and create a local co-ordinate system

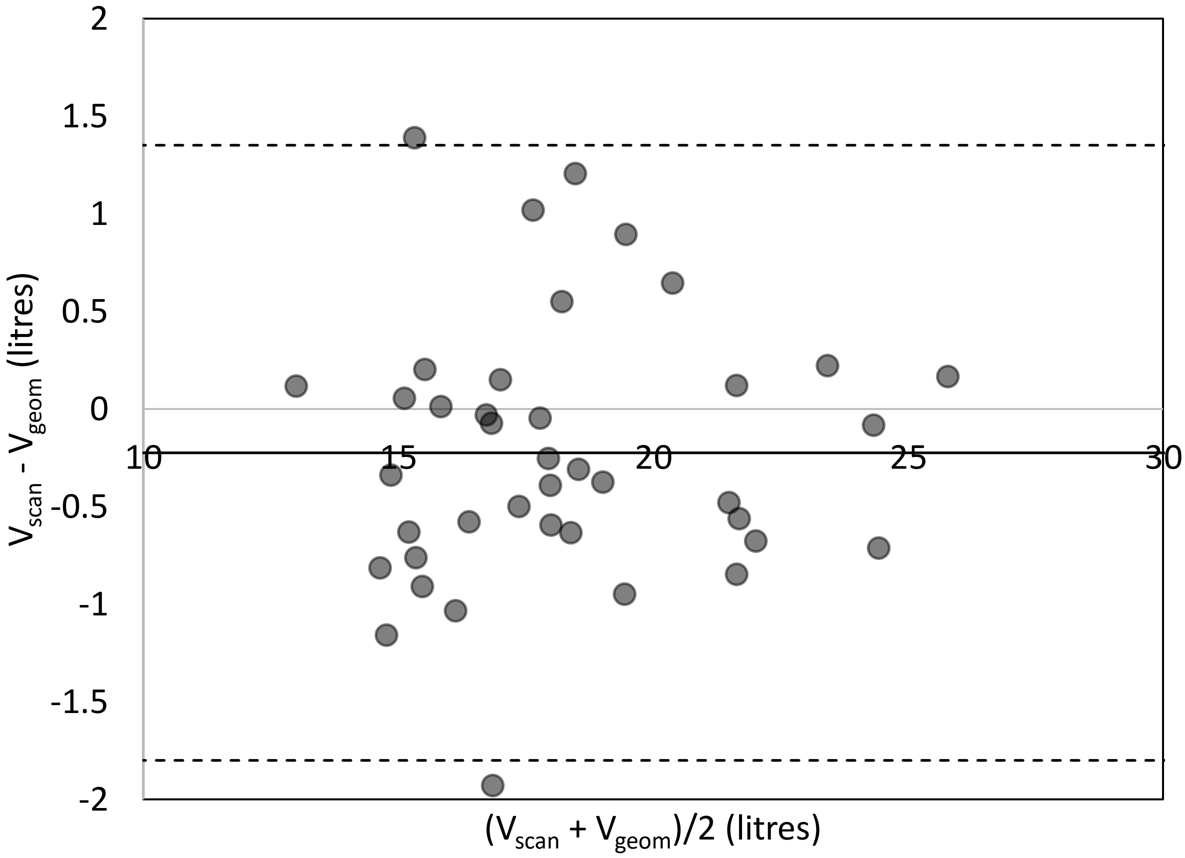

Figure 4. Limits of agreement between scan-derived volume and Yeadon-derived volume.

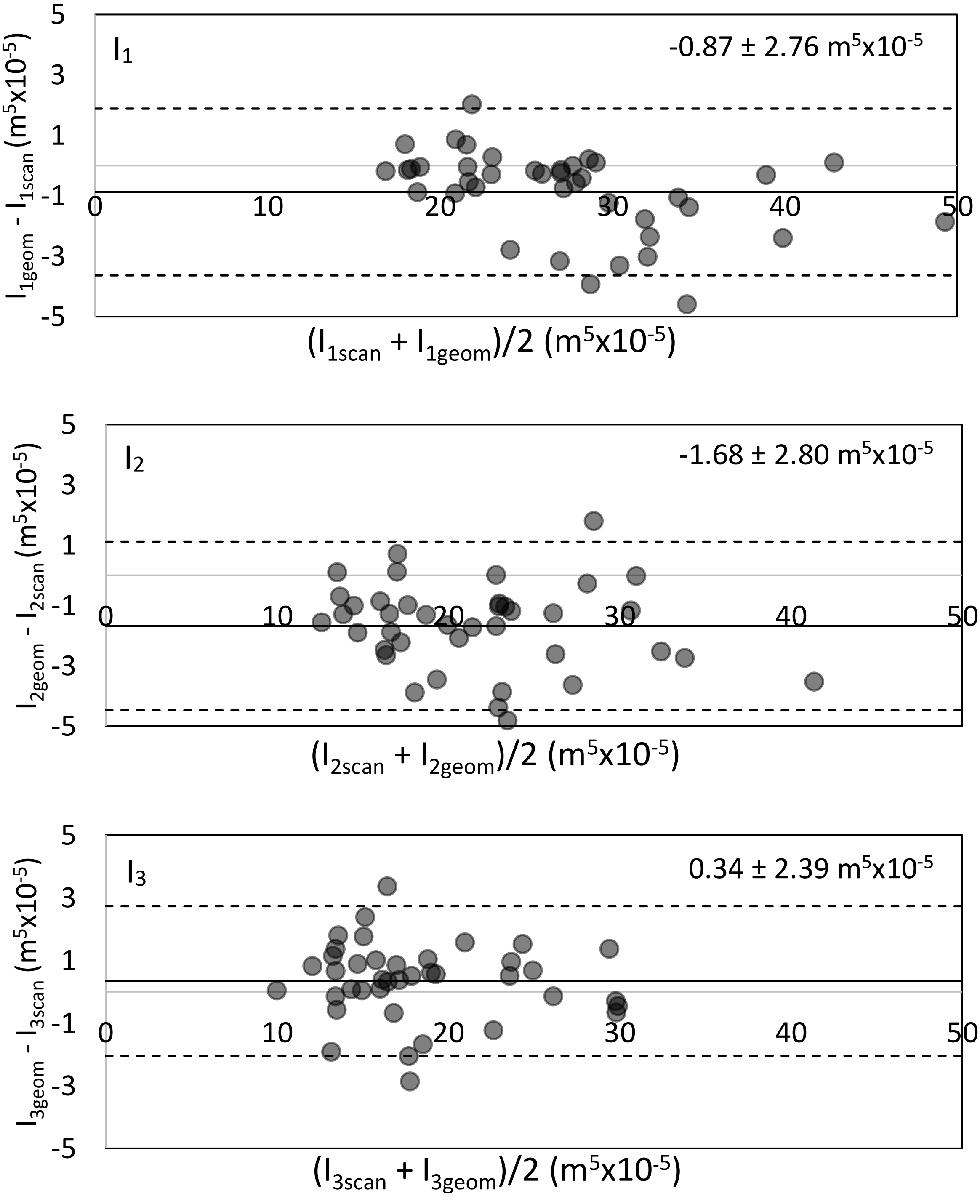

Figure 5. Agreement in Principal moments of volume between scanning and geometric modelling. The limits of agreement are not included on the plot due to their relatively large size compared to individual plot points.

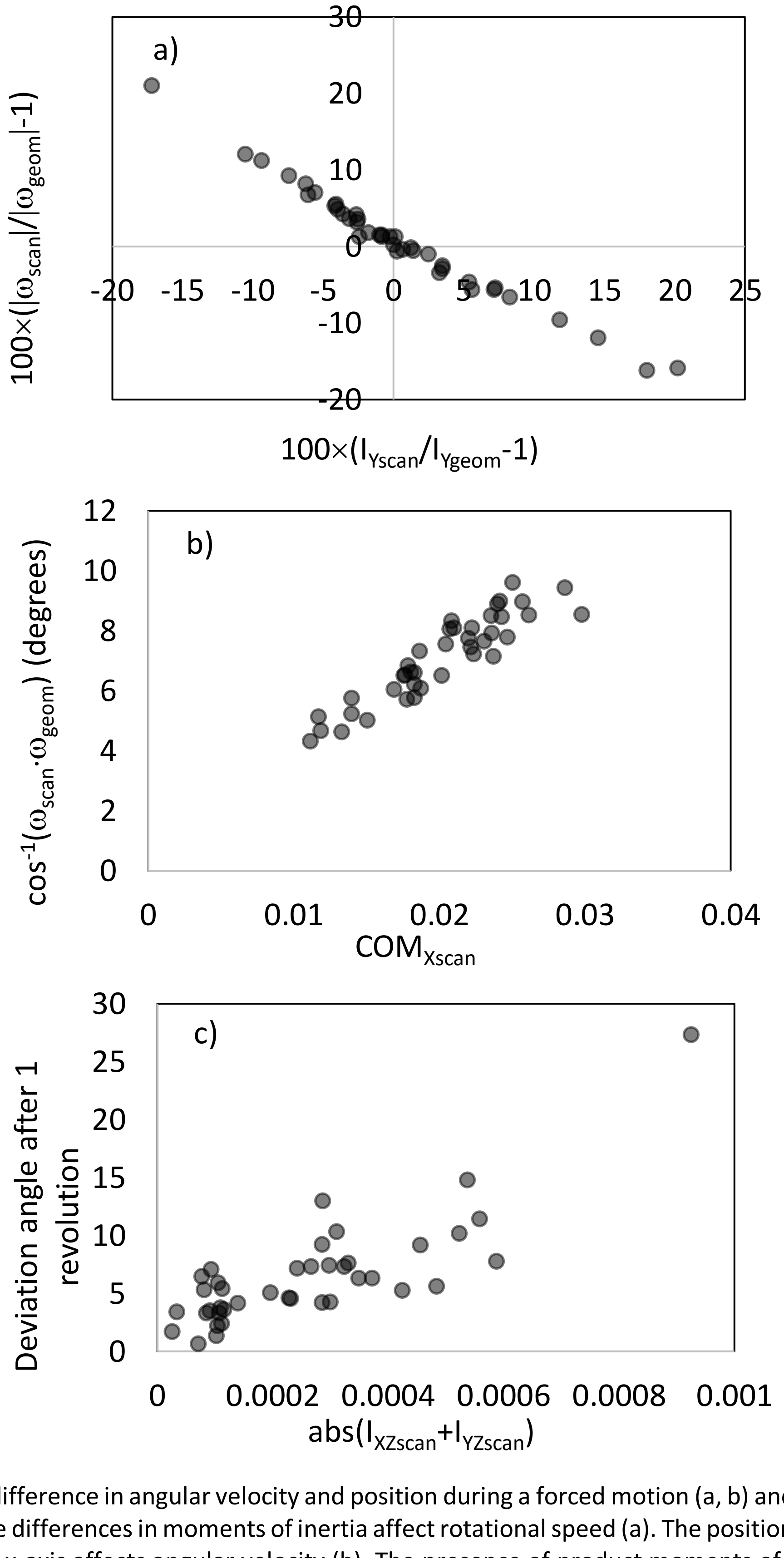

Figure 6. The difference in angular velocity and position during a forced motion (a, b) and free rotation (c). Percentage differences in moments of inertia affect rotational speed (a). The position of the centre of mass in the x-axis affects angular velocity (b). The presence of product moments of inertia causes angular deviations (c).

Tables:

Parameter	Scan			Geometric		
	Mean	Range	C.R	Mean	Range	C.R
Volume (l)	18.15	13.06-25.87	1.12	18.37	12.95-25.71	0.96
Centre of Mass (mm)						
X	20.20	11.15-29.80	3.95	0.00		0.00
Y	159.22	131.45-191.76	7.47	160.12	131.86-191.45	6.47
Z	0.49	-7.28-4.67	2.43	0.00		0.00
Principal Moments of Volume (m^5x10^{-5})						
1	28.00	17.00-50.00	3.00	26.81	16.77-48.38	2.36
2	22.00	13.00-43.00	2.60	20.81	11.84-39.62	2.62
3	18.00	10.00-30.00	1.80	19.00	10.00-30.09	1.19

Table 1. A summary comparison of the volumetric parameters calculated using each method.

Euler Angle (ZXY)	Mean	Range	C.R
α	11.65	5.67-31.70	2.74
β	1.93	-2.84-7.51	2.48
γ	10.31	0.74 – 95.83	13.34

Table 2. A summary of the Euler angles describing the relative orientations of the principal axes as measured by the geometric and 3D scanning method.

	Volume (l)		Centre of Volume (mm)				Principal moments of volume (m^5x10^{-5})						Principal axis orientation (°)		
Participant			COV_X	COV_Y		COV_Z	I1		I2		I3		α	β	γ
	Scan	Geometric	Scan	Scan	Geometric	Scan	Scan	Geometric	Scan	Geometric	Scan	Geometric	Scan	Scan	Scan
1	19.08(0.29)	17.88(0.25)	18.73(3.34)	175.17(1.51)	170.68(3.91)	2.55(1.56)	30.72(0.83)	26.78(0.69)	25.12(1.18)	20.73(0.61)	19.22(0.43)	16.34(0.29)	10.95(1.87)	-1.37(0.9)	1.98(4.63)
2	20.71(0.53)	20.07(0.64)	13.99(1.75)	151.78(5.19)	153.38(10)	1.48(2.66)	33.39(1.83)	31.01(2.69)	25.89(1.79)	21.08(1.83)	23.27(0.53)	22.04(0.89)	13.86(2.03)	-1.47(0.71)	4.31(7.8)
3	17.77(1.25)	17.82(0.85)	24.71(5.54)	175.48(10.06)	178.15(8.98)	1.36(2.14)	28.47(3.63)	28.04(3.31)	24.29(3.74)	23.1(3.11)	16.01(1.47)	16.09(0.81)	5.68(2.34)	0.56(2.07)	0.74(1.72)
4	25.87(1.33)	25.71(0.88)	29.8(1.87)	191.76(3.14)	191.45(1.8)	0.31(1.5)	50.24(3.69)	48.38(1.45)	43.16(2.93)	39.62(1.14)	30.15(3)	29.48(1.42)	6.94(0.12)	2.65(0.68)	1.11(3.11)
5	15.62(0.37)	15.42(0.47)	25.72(3.99)	158.66(7.08)	154.13(3.32)	2.28(3.08)	21.37(1.44)	20.44(1.29)	17.55(0.68)	15.07(0.98)	13.8(0.57)	13.22(0.55)	7.55(2.09)	1.81(1.53)	5.64(2.16)
6	18.49(0.72)	17.94(0.63)	28.65(3.16)	168.69(2.52)	171.3(3.17)	-2.61(3.4)	30.43(1.64)	29.19(1.17)	25.09(1.67)	21.22(0.93)	17.17(1.02)	16.48(0.92)	10.93(0.75)	4.39(0.55)	3.51(4.06)
7	21.41(0.71)	21.97(0.33)	16.93(3.76)	161.56(6.74)	160.65(4.51)	3.94(5.39)	35.17(2.28)	33.78(1.82)	27.59(1.92)	24.98(0.73)	24.62(1.12)	25.29(0.46)	13.71(2.48)	-1.53(2.83)	3.63(10.43)
8	19.91(0.43)	19.02(0.23)	23.72(5.38)	185.6(7.49)	188.76(7.57)	-0.05(1.96)	33.58(2.64)	30.55(1.62)	29.1(2.39)	25.47(0.75)	19.37(0.68)	17.69(0.74)	9.81(1.21)	3.17(1.17)	0.92(2.39)
9	18.16(0.83)	17.14(1.04)	13.33(0.68)	163.12(2.33)	165.9(3.33)	0.16(2.05)	28.57(1.52)	25.39(1.13)	21.09(1.16)	17.63(1.6)	18.73(1.67)	16.67(1.58)	10.51(0.32)	1.89(1.07)	8.4(3.16)
10	15.16(1.27)	15.1(0.77)	18.65(6.52)	142.23(4.32)	141.48(7.35)	0.54(1.39)	19.16(2.46)	18.28(1.35)	15.67(2.35)	13.78(1.97)	13.5(1.73)	13.35(0.88)	13.47(1.63)	3.1(3.52)	5.48(4.69)
11	16.02(0.8)	14.64(0.37)	26.17(4.29)	170.7(3.45)	171.92(0.45)	4.66(3.1)	25.48(1.59)	22.69(1.32)	19.99(1.43)	16.1(0.89)	14.15(1.17)	12.23(0.45)	5.67(0.34)	-1.72(0.84)	10.18(2.94)
12	21.68(0.98)	22.36(1.19)	18.32(3.68)	178.72(6.43)	181.86(3.72)	-2.62(1.94)	39.09(3.03)	38.78(2.94)	31.26(2.64)	30.08(3.61)	23.22(1.64)	24.16(1.56)	7.65(0.77)	4.37(1.63)	4.08(5.32)
13	24.29(2.96)	24.38(2.24)	23.1(1.62)	168.08(13.73)	166.93(10.97)	3.13(3.65)	41.12(8.75)	38.72(5.2)	33.69(7.4)	31.16(7.83)	30.15(5.34)	29.69(2.99)	12.38(0.64)	1.15(2.66)	8.53(9.98)
14	21.71(0.87)	21.59(0.4)	24.16(3.57)	146.94(2.3)	145.62(3.16)	-0.19(1.81)	32.11(1.57)	28.79(0.36)	26.76(1.66)	25.5(1.96)	26.21(1.88)	26.05(0.61)	22.16(1.99)	3.33(1.69)	95.83(63.84)
15	17.79(1.45)	18.19(2.07)	22.24(1.44)	151.44(12.04)	152.28(5.01)	0.39(4.35)	26.08(3.77)	25.79(3.81)	20.8(3.47)	19.14(4.42)	17.63(1.87)	18.12(2.37)	10.99(1.58)	4.62(3.13)	3.97(4.42)
16	21.25(2.28)	21.73(1.38)	20.2(0.2)	172.89(12.15)	172.18(9.61)	0.66(0.94)	34.36(7.51)	33.3(4.43)	28.26(5.27)	27.99(3.97)	23.35(4.03)	23.85(1.72)	9.4(2.07)	4.91(1.19)	1.61(3.28)
17	18.97(0.62)	19.92(0.67)	18.32(1.82)	157.04(0.8)	160.96(3.16)	4.09(1.63)	29.02(1.15)	29.12(0.89)	22.81(1.59)	22.81(1.33)	20.19(0.71)	21.76(0.91)	9.26(1.79)	1.81(3.58)	5.68(7.02)
18	21.22(1.4)	22.07(0.43)	22.02(3.7)	158.87(6.18)	157.07(4.29)	1.02(0.56)	32.79(3.77)	31.01(2.3)	27.63(3.35)	29.41(0.91)	23.59(2.5)	25.1(0.29)	17.22(2.99)	1.04(5.7)	5.81(10.71)
19	23.54(0.83)	23.32(0.8)	23.59(6.23)	154.32(6.4)	150.34(3.44)	-1.98(5.44)	36.64(1.45)	32.04(1.42)	31.01(2.06)	30.98(4.02)	29.93(1.5)	29.63(1.67)	31.7(8.77)	3.12(8.52)	2.07(4.12)
20	15.85(1.5)	15.84(1.49)	18.06(4.16)	154.48(16.66)	156.75(13.73)	1.77(2.02)	21.95(4.19)	21.4(4.24)	17.63(3.96)	15.75(3.28)	14.31(1.71)	14.37(1.37)	13.66(3.1)	-0.71(1.82)	1.16(1.85)
21	17.08(0.29)	16.93(0.75)	17.79(3.32)	174.38(0.54)	178.94(4.76)	1.28(0.51)	27.14(0.2)	26.9(1.16)	22.28(0.41)	20.55(0.93)	14.95(0.39)	14.98(0.94)	5.91(1.49)	-0.83(1.54)	1.2(1.14)
22	17.7(0.88)	18.3(0.96)	17.57(1.16)	151.19(2.98)	153.76(2.05)	2.25(3.2)	25.62(1.28)	25.45(1.49)	19.38(0.78)	18.06(1.66)	18.29(2.07)	19.33(1.29)	10.65(0.81)	-0.22(3.13)	16.18(29.3)
23	16.71(0.99)	16.75(0.79)	24(0.99)	150.64(4.3)	153.48(0.42)	2.59(2.52)	22.46(2.35)	21.74(2.19)	18.34(1.84)	16.12(1.86)	16.32(1.52)	16.63(0.83)	16.45(1.94)	1.04(1.28)	6.58(5.82)
24	16.8(0.3)	16.88(0.3)	21.02(1.55)	142.44(0.53)	144.69(2.19)	0.94(1.88)	23.16(0.33)	22.86(0.76)	17.72(0.34)	15.06(0.45)	16.97(0.67)	17.33(0.4)	11.41(2.43)	-0.19(1.48)	23.76(11.06)
25	14.24(0.83)	15.06(0.99)	20.86(3.52)	139.53(5.77)	140.92(6.45)	-0.14(1.64)	18.4(1.61)	18.29(1.92)	14.04(1.54)	13.33(1.96)	12.72(1.13)	13.86(1.25)	14.31(2.96)	2.14(0.92)	7.18(5.41)
26	18.83(0.45)	19.21(0.38)	24.28(1.56)	160.05(2.84)	159.01(0.21)	1.18(2.06)	27.56(1.28)	26.8(0.72)	23.49(0.89)	22.47(1.33)	18.69(0.81)	19.3(0.41)	15.16(0.25)	1.98(1.6)	4.3(1.8)
27	14.7(0.48)	15.04(0.82)	25.05(5.86)	142.08(7.89)	144.13(7.78)	-0.39(0.41)	18.22(1.38)	18.07(2.22)	15(1.37)	13.99(1.47)	13.11(0.62)	13.77(0.61)	7.68(3.65)	7.51(1.5)	22.22(26.16)
28	18.39(2.3)	18.7(1.73)	20.48(5.22)	152.96(11.02)	153.88(6.83)	4.67(0.5)	27.11(5.21)	26.96(3.39)	21.68(4.73)	19.59(3.52)	19(3.67)	19.56(2.5)	9.04(3.79)	-1.32(1.93)	3.92(7.05)
29	14.9(0.72)	15.54(0.27)	22.18(8.96)	167.51(6.65)	166.83(5)	-1.7(1.18)	21.64(1.64)	21.6(1.08)	18.15(1.32)	17.16(0.43)	11.68(0.96)	12.49(0.35)	9.71(1.25)	3.81(1.48)	3.88(2.71)
30	17.13(0.78)	17.63(0.89)	15.08(2.38)	173.78(6.43)	178.66(3.98)	-3.42(1.25)	27.72(2.4)	27.71(2.3)	23.47(2.12)	22.52(2.41)	14.3(0.99)	15.18(0.84)	7.44(1.05)	4.34(1.07)	5.04(4.06)
31	14.19(0.47)	15.35(0.26)	14(2.38)	138.48(3.09)	137.86(5.45)	-3.06(0.38)	17.64(1.24)	18.33(0.89)	13.47(1.05)	13.57(0.52)	12.71(0.49)	14.5(0.24)	10.18(0.94)	3.79(1.64)	23.89(13.68)
32	18.07(0.99)	18.7(1.11)	23.63(4.24)	167.09(4.95)	171.86(5.74)	-2.79(2.96)	28.2(2.84)	27.61(2.65)	23.88(2.75)	22.82(2.69)	16.56(1.18)	17.4(1.33)	10.44(1.29)	4.9(2.1)	4.06(2.66)
33	24.08(0.76)	24.79(0.59)	18.3(2.59)	175.72(4.32)	173.56(3.8)	-7.28(0.65)	42.82(2.99)	42.91(2.94)	35.2(2.9)	32.45(1.55)	28.73(0.94)	30.09(0.63)	9.62(1.27)	3.4(2.51)	3.68(4.69)
34	17.82(0.42)	18.08(0.08)	22.39(1.56)	172.87(4.97)	172.27(5.9)	1.09(2.24)	28.55(1.55)	28.74(1.61)	23.66(1.27)	21.97(1.07)	15.98(0.46)	16.36(0.09)	8.06(0.68)	0.95(1.21)	1.21(0.89)
35	15.02(1.32)	15.93(0.95)	11.72(6.31)	131.45(11.86)	131.86(12.39)	-0.22(0.68)	18.9(2.75)	18.85(2.89)	14.52(1.99)	13.23(1.98)	13.97(2.26)	16.34(1.18)	25.43(8.4)	0.92(0.65)	90.46(15.08)
36	15.61(1.61)	16.65(0.91)	17.67(2.67)	151.99(10.94)	152.65(9.35)	0.94(2.21)	21.22(3.66)	21.89(1.46)	16.97(3.3)	17.08(5.81)	14.2(2.1)	15.95(0.7)	10.94(1.53)	2.69(0.86)	2.38(3.5)
37	15.9(0.59)	17.83(0.7)	20.73(5.45)	142.14(6.42)	143.28(1.37)	-0.66(1.84)	20.84(1.32)	22.87(0.92)	16.71(0.75)	17.41(1.55)	14.79(0.98)	18.14(1.17)	10.35(4.79)	4.48(4.41)	7.59(2.91)
38	13.06(0.82)	12.95(0.67)	17.88(4.73)	147.3(3.07)	151.25(5.38)	-1.13(2.85)	16.97(1.48)	16.77(1.12)	13.41(1.45)	11.84(1.01)	9.99(0.93)	10.03(0.72)	8.93(1.25)	-2.84(0.84)	3.42(8.73)
39	16.11(0.74)	16.69(0.77)	11.9(1.15)	148.73(7.2)	150.83(6.49)	2.74(3.99)	22.91(1.94)	23.19(2.27)	17.22(1.76)	15.94(1.82)	15.28(0.9)	16.28(0.71)	11.04(1.61)	3.33(2.21)	9.25(8.56)
40	14.98(1.51)	15.74(1.72)	11.15(5.84)	151.01(15.36)	153.17(13.68)	1.85(0.74)	20.49(4.03)	21.36(4.42)	16.47(3.78)	15.6(4.29)	12.77(1.57)	14.12(1.57)	11.09(3.53)	0.78(1.29)	4.3(2.1)
Mean	18.15(1.12)	18.37(0.96)	20.20(3.95)	159.22(7.47)	160.12(6.47)	0.49(2.43)	28.00(3.00)	26.81(2.36)	22.00(2.60)	20.81(2.62)	18.00(1.80)	19.00(3.20)	11.65(2.74)	1.93 (2.48)	10.48 (13.34)

Table Supp1. The volumetric parameters for all participants, as measured using the geometric and 3D scanning methods. Shown as: mean(C.R) of 3 repeats.